Frontiers of Materials Science

Electronic Supplementary Material

Preparation of Pd nanoparticle-modified $FeWO_4$ hollow spheres for highly selective hydrogen sulfide and acetone detection

Chen Chen[1], Jie Chang (✉)[2], Yu Sun[3], Areeje Fatima[3], and Jiarui Huang (✉)[3]

1 School of Materials Science and Engineering, Tongling University, Tongling 244000, China
2 Anhui Engineering Research Center of Highly Reactive Micro-Nano Powders, School of Materials and Environmental engineering, Chizhou University, Chizhou 247000, China
3 Key Laboratory of Functional Molecular Solids of the Ministry of Education, Anhui Laboratory of Molecule-Based Materials, College of Chemistry and Materials Science, Anhui Normal University, Wuhu 241002, China

E-mails: changjie@czu.edu.cn (J.C.), jrhuang@ahnu.edu.cn (J.H.)

1 Preparation of $(NH_4)_3PW_{12}O_{40}·9.5H_2O$ dodecahedra

Ammonium tungsten phosphate hydrate ($(NH_4)_3PW_{12}O_{40}·9.5H_2O$) dodecahedra were prepared via a liquid-phase reaction. Briefly, phosphotungstic acid ($H_3PW_{12}O_{40}$, 3.6 g) and ammonium bicarbonate (0.295 g) were separately dissolved in 95 mL of deionized water. Subsequently, 95 mL of ammonium bicarbonate solution was gradually mixed with the $H_3PW_{12}O_{40}$ solution while stirring consciously in a water bath at 95°C. After 30 min of stirring, a milky suspension was observed. The suspension was centrifuged and repeatedly rinsed with deionized water to eliminate contaminants, followed by drying at 80 °C for 24 h to yield $(NH_4)_3PW_{12}O_{40}·9.5H_2O$ powder.

2 Material characterization

The products were characterized by X-ray diffraction (XRD, Shimadzu XRD-6000) using high-intensity Cu Kα radiation with a wavelength of 1.54178 Å, as well as field-emission scanning electron microscopy (FESEM, Hitachi S-4800, operated at 5 kV), high-resolution transmission electron microscopy (HRTEM, JEOL-2010 TEM) with an acceleration voltage of 200 kV, and N_2 adsorption–desorption isotherm measurements (Nova 2000E). The pore-size distribution was determined from desorption branch of the isotherm using the Barrett–Joyner–Halenda (BJH) method. X-ray photoelectron spectroscopy (XPS, ESCALAB 250) and solid UV–Vis spectrophotometer (UV-Vis-3010, Hitachi) were also performed. The element distribution of products was determined by energy dispersive spectroscopy (FESEM, Hitachi S-4800, operated at 15 kV). The elemental mapping of the sample was obtained by energy dispersive spectroscopy (HRTEM, JEOL-2010 TEM) with an acceleration voltage of 200 kV.

3 Gas-sensor fabrication and sensing tests

The gas-sensor fabrication was very similar to those in our previous report. First, 0.1 g of Pd/$FeWO_4$ hollow spheres was dispersed in 0.3 mL ethanol solution to obtain a homogeneous suspension. Then the outer surface of an aluminum tube-like substrate with a pair of Au electrodes attached was uniformly coated by the suspension. The treated-substrate was dried for 2 h at room temperature and then annealed for another 2 h at 200 °C. This annealing process will make the structure of sensing film stable. After that, a small Ni–Cr alloy coil heater was inserted into the tube in order to provide the working temperature of the gas sensor. Figure S1 illustrates the schematic diagram of the gas sensor. Moreover, the sensor was kept at the working temperature (250 °C) for 2 d to improve the long-term stability. In this study, a stationary-state gas distribution method was adopted to test the gas response. The sensor response measurement was performed on an electrochemical workstation (CHI-660E, Shanghai Chenhua Instruments Co., Ltd.). To detect gases, a certain amount of various headspace vapors was injected into a 1000 mL of test chamber using a syringe and mixed with air. As for the sample gases, H_2S (pure hydrogen sulfide gas) and H_2 (pure hydrogen gas) were used in the gas sensing measurement. All other VOCs vapors, such as ethanol, methanol, acetone, and toluene, came from the headspace vapors of the pure chemical regents at 28 °C under ambient pressure. The electrical resistance of the gas sensor was determined by measuring the electric current that flowed when a potential difference of 0.6 V was applied between Au electrodes. The sensor response was defined as $S = R_a/R_g - 1$ (reducing gases), where, R_a is the resistance of the sensor in dry air, and R_g is that in the dry air mixed with detected gases. In our measurement system, the response also can be calculated by the following equation: $S = I_g/I_a - 1$, where I_g and I_a were the output currents in test gas and air, respectively. The response or recovery time was expressed as the time required for the sensor output to reach 90% saturation after applying or switching off the gas in a step function. The optimal working temperature of the as-fabricated sensor was investigated, and the following tests were performed at the optimal operating temperature.

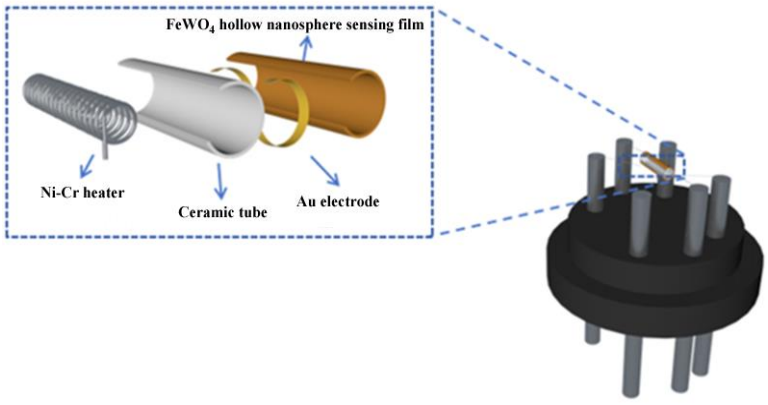

Fig. S1 Schematic diagram of a gas sensor device.

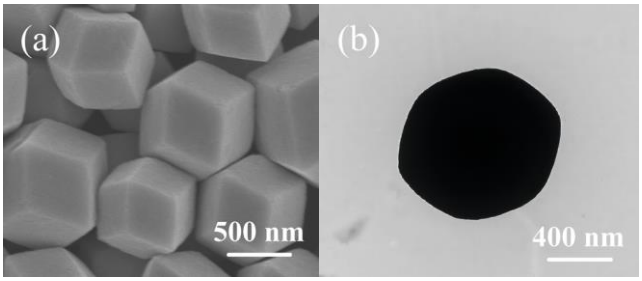

Fig. S2 (a) SEM and **(b)** TEM images of $(NH_4)_3PW_{12}O_{40}\cdot 9.5H_2O$ dodecahedra.

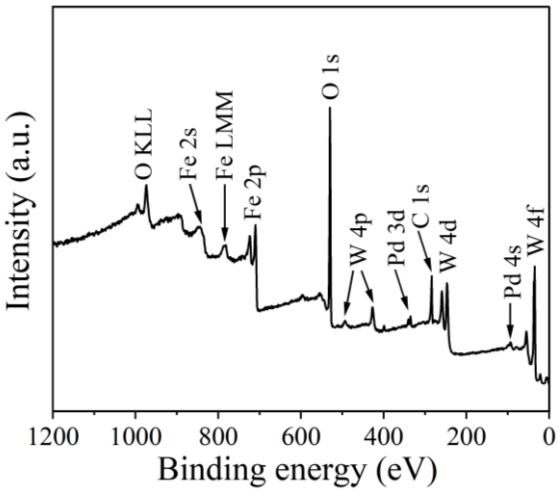

Fig. S3 XPS survey spectrum of 3-Pd/$FeWO_4$ hollow spheres showing the characteristic signals of Pd, Fe, W, O, and C.

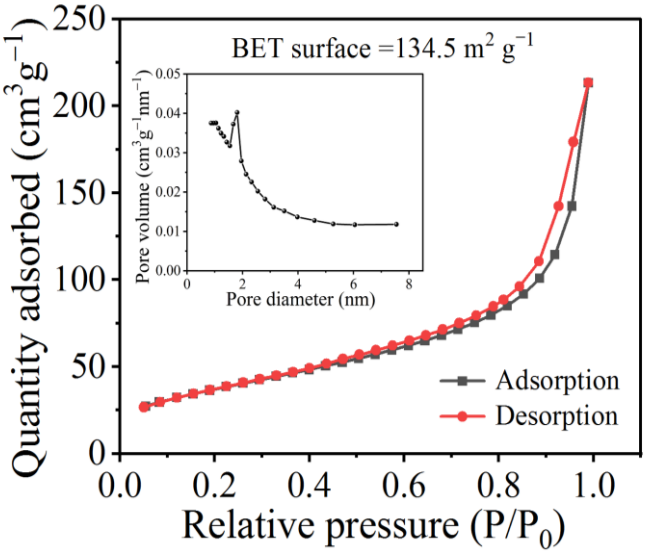

Fig. S4 Nitrogen adsorption/desorption curves of 3-Pd/$FeWO_4$ hollow spheres. Inset is corresponding pore size distribution curve.

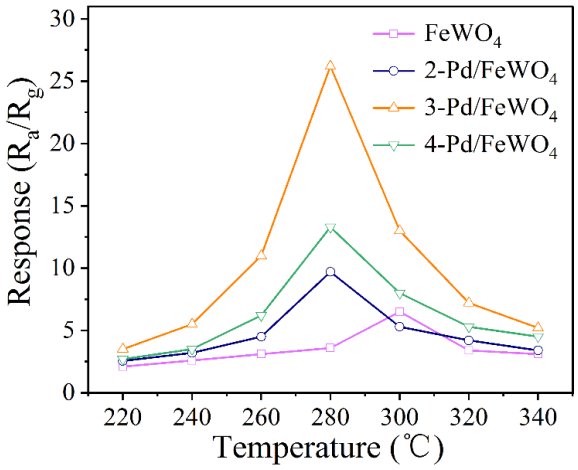

Fig. S5 Response of the $FeWO_4$, 2-Pd/$FeWO_4$, 3-Pd/$FeWO_4$, and 4-Pd/$FeWO_4$ hollow sphere sensors to 100 ppm acetone gas at different operating temperatures.

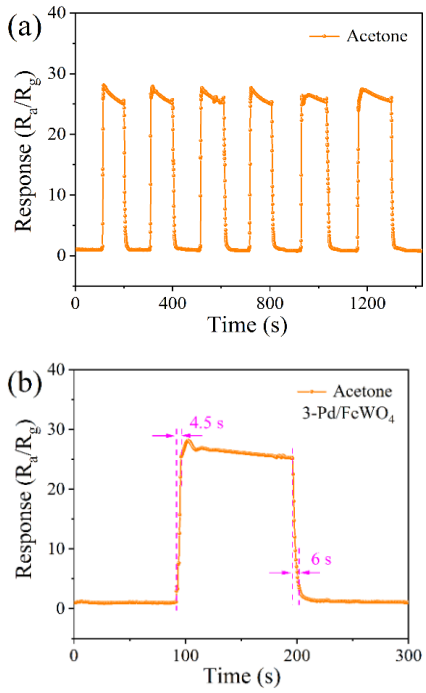

Fig. S6 (a) Repetitive response curve to 100 ppm acetone and **(b)** real-time response curve to 100 ppm acetone of the 3-Pd/$FeWO_4$ hollow sphere sensor.

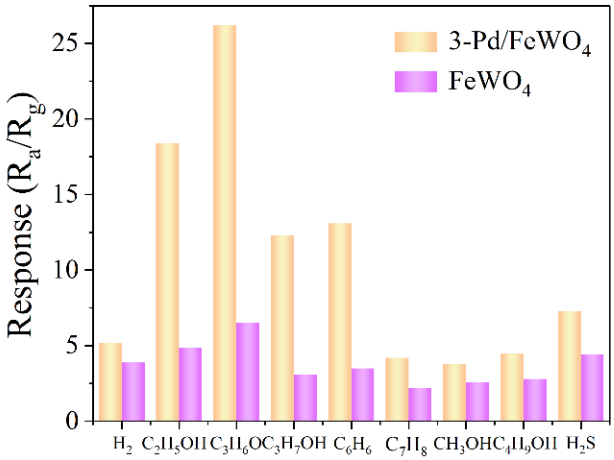

Fig. S7 Comparison of the detection sensitivities of the $FeWO_4$ and 3-Pd/$FeWO_4$ hollow sphere sensors for different gases at their optimal operating temperatures.

Table S1 Comparison of acetone sensing properties of 3-Pd/$FeWO_4$ hollow sphere sensor in this work with some related sensing materials previous reported

Gas-sensing material	Concentration /ppm	Operating temperature/°C	(Response time/ recovery time)/s	Response	Ref.
Co_3O_4 nanoparticles	100	200	43/92	8.6	[7]
Bi_2WO_6 nanoflowers	50	290	–/–	10.1	[23]
$DyFeO_3$ powder	2	190	42/44	3.8	[52]
CeO_2–WO_3 nanowires	0.5	250	34/68	1.3	[53]
Ca-doped $YbFeO_3$ nanomaterials	3	230	16/47	5.0	[54]
$BiFeO_3$ nanoparticles	10	350	-/-	12	[55]
3-Pd/$FeWO_4$ hollow spheres	100	280	4.5/6.0	26.2	This study

Table S2 Comparison of hydrogen sulfide sensing properties of 3-Pd/$FeWO_4$ hollow sphere sensor in this work with some related sensing materials previous reported

Gas-sensing material	Concentration /ppm	Operating temperature/°C	(Response time/ recovery time)/s	Response	Ref.
Fe_2O_3 nanoboxes	5	50	806/1100	2.58	[56]
Ru-Fe_2O_3 nanoboxes	100	200	8/34	32.6	[57]
ZnO/Fe_2O_3 nanoplates	100	250	19.1/156	130	[58]
TiO_2@Fe_2O_3 nanorods	200	300	~150/150	7.4	[59]
$SnSe_2$/WO_3 composite	10	25	136/459	1.34	[12]
Pd-WO_3 microspheres	5	190	2/58	242	[45]
3-Pd/$FeWO_4$ hollow spheres	10	25	206/237	2.3	This study